Journal of Vibration and Control
http://jvc.sagepub.com

Sliding Mode Control of a Finger for a Prosthetic Hand

Nurkan Yagiz, Yunus Ziya Arslan and Yuksel Hacioglu

Journal of Vibration and Control 2007; 13; 733
DOI: 10.1177/1077546307072352

The online version of this article can be found at:
http://jvc.sagepub.com/cgi/content/abstract/13/6/733

Published by:
SAGE Publications
http://www.sagepublications.com

Sliding Mode Control of a Finger for a Prosthetic Hand

NURKAN YAGIZ
YUNUS ZIYA ARSLAN
YUKSEL HACIOGLU
Department of Mechanical Engineering, Faculty of Engineering, Istanbul University, 34320 Avcilar, Istanbul, Turkey, (nurkany@istanbul.edu.tr)

(Received 10 April 2006; accepted 23 August 2006)

Abstract: A prosthetic finger model, intended to imitate a real human hand and for use in replacing the real index finger of an amputee, is designed using tendons instead of joint motors. A dynamic model of the prosthetic finger model is developed, and a non-chattering robust sliding mode control is applied to make the model follow a certain trajectory. Trajectory planning of the finger model is based on images of the closing motion of a human hand, and time varying reference joint angles are obtained using these images. The robustness of the controller is confirmed by introducing an unexpected sudden joint friction induced in the prosthetic finger.

Keywords: Prosthetic finger, prosthetic hand, sliding mode control, trajectory planning, tendon forces.

1. INTRODUCTION

Much research has been carried out into the biomechanical and neuro-physiological properties of the muscle systems of the human hand, in order to define the relationships between muscular contractions and variable dynamic movements (Gregory, 2002). The need to determine the musculoskeletal forces applied to body segments arises from the desire to improve the conditions of handicapped people who need prosthetic limbs. Various prosthetic hands have been designed and developed over the last fifteen years to meet the requirements of amputees (Jones, 1997). Unfortunately, no prosthesis design has matched the functional features of the human hand, which has magnificent mechanical properties (Bundhoo and Park, 2005). Today's widely used prosthetic hands typically have restricted open/grasp movement properties (Jones, 1997). Artificial hands that are more flexible and functional are still under investigation (Morita et al., 2000, 2001). There are two main problems to be solved in constructing a highly advanced hand prosthesis. These are the production of a mechanical design that will allow sufficient freedom of movement, and the creation of robust controllers that can handle such a complicated mechanical design.

Journal of Vibration and Control, **13(6):** 733–749, 2007 DOI: 10.1177/1077546307072352

Figures 1, 2, 5 appear in color online: http://jvc.sagepub.com

Movement of the human body is performed by muscles, which apply forces to the skeleton via tendons. In the literature, the motion mechanism of the human hand is widely adopted, with robot and prosthetic hand designs intended to mimic natural movements. Pollard and Gilbert (2002) examined the tendon arrangements of the human hand with the aim of optimizing the total muscle force requirements of robot hands. It can be concluded from this study that a robot hand can have a force capability very similar to that of the human hand. Li et al. (2000) determined the forces produced by extrinsic muscles and intrinsic muscle groups of individual fingers by using two two-dimensional biomechanical models during isometric contractions. Bundhoo and Park (2005) designed a biomimetic finger actuated by a type of artificial muscle made from shape memory alloys. Weghe et al. (2004) constructed an anatomically-correct test bed of the human hand to evaluate its mechanism, function and control. Tsang et al. (2005) presented a realistic skeletal musculo-tendon model of the human hand and forearm that permits prediction of hand and finger position from a given set of muscle activations. Fukaya et al. (2000) designed a new humanoid-type hand (called TUAT/Karlsruhe Humanoid Hand) with human-like manipulation abilities for use with the humanoid robot ARMAR (Asfour et al., 1999).

In recent years, much work has been done with tendon driven mechanisms which consist of belt pulley connections, a rotor assembly and a serial manipulator. Jacobsen et al. (1990) used a derivative and integral controller to control a double actuated single joint, driven by tendons. Kawanishi et al. (2000) designed a tendon driven four degree of freedom (DoF) robot finger and used a fuzzy logic controller for position control of the fingertip. Elasticity of the tendons was also taken into account. Hristu et al. (1994) compared a fuzzy logic controller with a traditional PID controller for use with a multifinger robot hand. The objective was to control both the position of the fingertip and the forces exerted on the fingertip, and the fuzzy logic controller outperformed the PID controller.

PID controllers are widely used in industrial robotics, because of their simplicity. On the other hand, this type of control is not efficient when there are parameter variations and external disturbances; for dealing with those, it is important to have a robust controller. Sliding mode control, as a special class of variable structure, is preferred in robotics and in a range of other applications because of its robustness. This control method has become widespread since its introduction by Utkin (1977). The basic idea is to drive the system state to the so-called sliding surface and then keep the system within a specified distance of this surface. Slotine and Sastry (1983) developed a sliding mode controller for control of time varying non-linear systems and applied this controller to a two-link manipulator, which is designed to handle variable loads in a flexible manufacturing system environment. Gao and Hung (1993) presented a new approach, called the reaching law method, for the design of variable structure controllers for non-linear systems. The approach was applied to a two-link robot arm to demonstrate its effectiveness. Cavallo and Natale (2004) proposed a control strategy based on a second order sliding manifold multiple-input multiple-output (MIMO) approach, which was used to design a robust multivariable linear controller. A six DoF manipulator was used as a test bed for experiments.

In this study, kinematic and dynamic analysis of the motion of a human finger as the hand is closed is carried out based on an approximate model of human hand anatomy. Then, a robust non-chattering sliding mode control is applied to this finger model to achieve the required trajectory. Because of the similarity of the kinematic structures of the bones in each finger, motion analysis is conducted for one finger only. Hence, in this study analyzing the

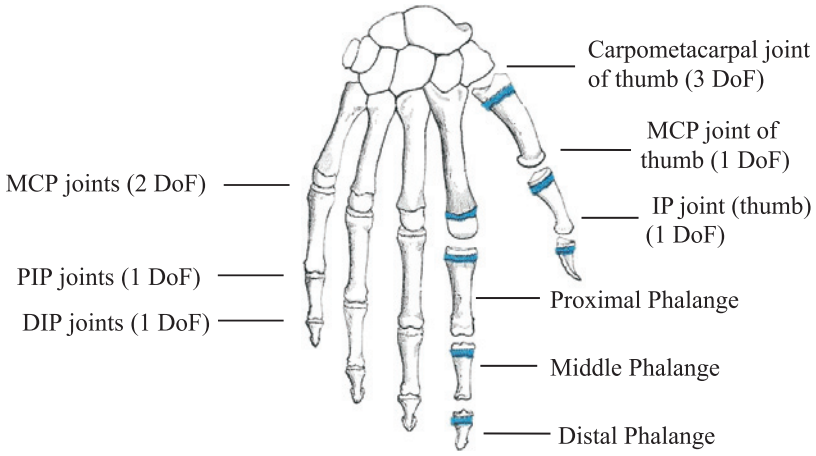

Figure 1. Joints of the human hand (Gray, 1858).

flexion movement of the human hand is reduced to examination of the motion of one finger. It is assumed that a finger can be represented by a series of links attached by joints in an anthropomorphic design. During the construction of the model, care was taken to insure that the bone dimensions, tendon attachment points, and tendon structures are similar to a real human hand. The joint angles during the closing motion are obtained from camera images of a real hand, and used to calculate the control forces applied to the bones via the tendons. This study is different from previous efforts which include motion analysis of the hand (Fukaya et al., 2000; Rohling and Hollerbach, 1994) in that the tendon forces required for tracking a specific trajectory are calculated using a sliding mode controller, which gives efficient and robust tracking performance in spite of parameter variations.

2. BIOMECHANICAL MODEL OF A HUMAN HAND

2.1. Anatomy and Tendon Configuration

The human hand is a highly articulated structure. The high functionality of the human hand is based on its numerous degrees of freedom (DoFs). The human hand has 23 DoFs, provided by 17 joints (LaViola, 1999). If three-dimensional movement is taken into consideration, this increases to 29 DoFs because of orientation and positional movement of the hand controlled by the wrist and arm. Figure 1 shows the joints of the hand.

The phalanges are the small bones that constitute the skeleton of the fingers and thumb. The nearest phalange to the hand body is the proximal phalange and the one at the far end of the each finger is the distal phalange. The distal interphalangeal (DIP) and proximal interphalangeal (PIP) joints each have 1 DoF (rotational movement), and the metacarpophalangeal (MCP) joint has 2 DoFs: adduction-abduction and rotational motion. The four fingers (index, middle, ring and little fingers) have similar structures in terms of kinematic and dynamic features. The thumb is different from the fingers in that it contains only two phalanges and

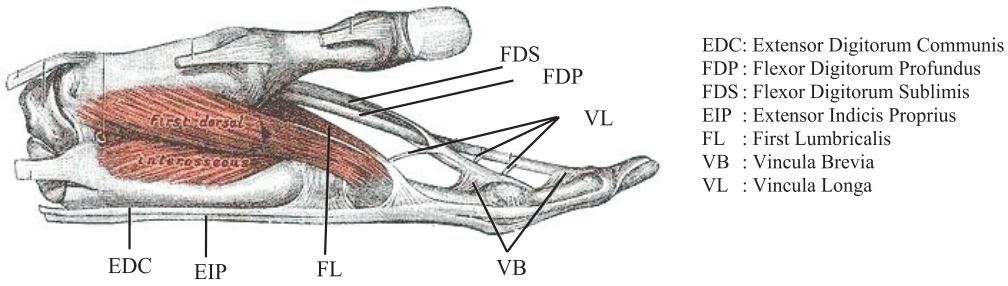

Figure 2. Tendons in the flexion and extension movements (Gray, 1858).

has 5 DoFs. The index finger has the greatest range of motion amongst the fingers; its range of extension/flexion movement is typically around 80° at the DIP joint, 110° at the PIP joint and 90° at the MCP joint. Abduction and adduction angles have been measured as 20° at the MCP joint in the index finger (Bundhoo and Park, 2005)

Muscles are only able to exert pulling effort, and muscle forces are transmitted to the finger bones via tendons. More than fifteen tendons extend from the forearm muscles to the hand. In the extension-flexion movement of the fingers, one set of muscles and tendons carries out the extension motion of the finger, and a different set of muscles and tendons produces the flexion motion (Figure 2).

Tendon configuration in the hand is complex and this sophisticated tendon arrangement contributes to the high functionality of human hand motion. Hand extensor tendons, which are on the back side of hand, straighten the fingers, and flexor tendons, on the palm side of the hand, bend the fingers. In this study, a 3 DoF rigid body chain mechanism is modeled that closely mimics the size and functionality of the human index finger. Tendon attachment points of the phalanges are reduced to three each on the palm and back sides of the hand, as shown in Figure 3.

2.2. Index Finger Model

The prosthetic finger model used in this study has three degrees of freedom. It consists of three links, which represent the proximal, middle and distal bones of the index finger of human hand. The physical model of the finger is shown in Figure 4.

F_1, F_2 and F_3 are the flexion forces and F_1', F_2' and F_3' are the extension forces. β_i $(i = 1, 2, 3)$ is the angle between the tendon forces and the phalanges. In the human hand, the skin tissue covers the finger bones and tendons, thus β_i attains only small values; in this study they are limited to 10° each.

M_i, I_i and L_i are the mass, mass moment of inertia and length of link i. a, b and c are the distances of the mass centers of the first, second and third links, respectively, from the center of the preceding joint. θ_i is the joint angle of the related link and b_i denotes the viscous friction at the joints. a_i is the distance of the tendon attachment point to the related joint and t_i is the diameter of the related link at this point. Numerical parameters of the model finger used are given in Appendix A.

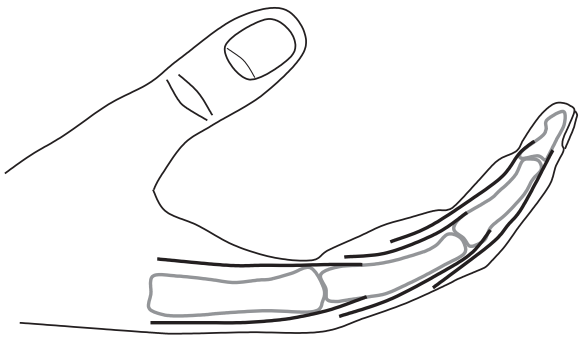

Figure 3. Simplified tendon arrangement of the index finger.

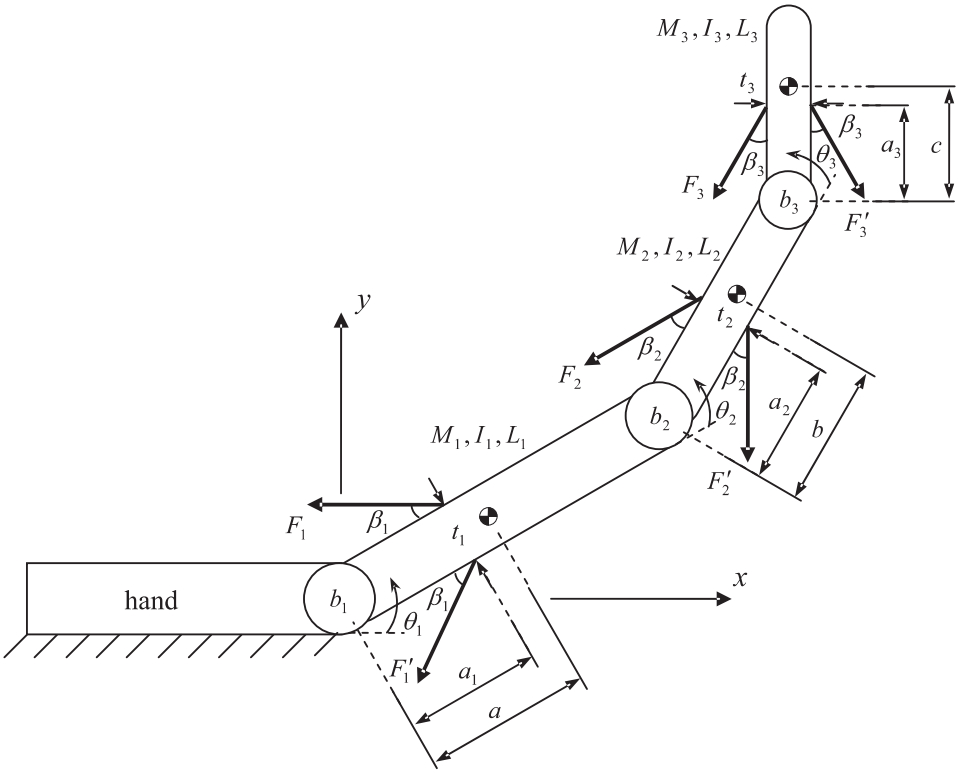

Figure 4. Prosthetic finger model.

The equations of motion are obtained using Lagrange equations as

$$[M(\theta)]\ddot{\theta} + \mathbf{C}(\theta, \dot{\theta}) + \mathbf{G}(\theta) = \mathbf{u} \tag{1}$$

where $[M(\theta)]$ is the $n \times n$ mass matrix of the finger, $\mathbf{C}(\theta, \dot{\theta})$ is an $n \times 1$ vector and includes the coriolis terms, centrifugal terms and undesired joint viscous frictions, $\mathbf{G}(\theta)$ is an $n \times 1$ vector of the gravity terms, and $\mathbf{u}$ is an $n \times 1$ vector of the generalized torque input produced by tendons on the phalanges; n is the number of degrees of freedom. The matrix and vector terms in equation (1) are given in Appendix A.

The tendon forces are obtained using the relation

$$\mathbf{F}_c = [J]^{-T}\mathbf{u} \tag{2}$$

where $[J]^{-T}$ is inverse transpose Jacobian (Craig, 1989), and $\mathbf{F}_c$ is the vector having the cartesian components of the tendon forces F_1, F_2, and F_3. $\mathbf{F}_c$, $[J]^T$, $\mathbf{u}$ and the tendon forces are given in Appendix B.

3. SLIDING MODE CONTROL

Sliding mode control, as a special class of variable structure systems, can be applied to non-linear systems effectively even in the presence of parameter variations and external disturbances. In these systems, states of the system are driven towards a sliding surface and constrained to stay on or near it. Thus there are two parts in the design stage of these controllers. First, a sliding surface is defined in the state space, and second, the control law, which is responsible for constructing and maintaining the sliding motion, is obtained.

The state space form of a non-linear dynamic system can be written as

$$\dot{\phi} = \mathbf{f}(\phi) + [B]\ \mathbf{u} \tag{3}$$

where $\phi = \left[\phi_1, \ldots, \phi_n, \phi_{n+1}, \ldots, \phi_{2n}\right]^T$.

The second half of the states are the time derivatives of the first half (i.e., state ϕ_{n+a} is the time derivative of state ϕ_a), and $2n$ is the total number of the states. $\mathbf{f}(\phi)$ is the vector including all nonlinear terms, and $[B]$ is the control input matrix. The sliding surface is defined as

$$S = \{\phi : \boldsymbol{\sigma}(\phi, t) = 0\}. \tag{4}$$

For a control system, the sliding surface can be selected to be

$$\boldsymbol{\sigma} = [G]\ \Delta\phi \tag{5}$$

where

$$\Delta\phi = \phi_r - \phi = \left[\mathbf{e}\ \ \mathrm{d}\mathbf{e}/\mathrm{d}t\right]^T \tag{6}$$

is the difference between the reference value and the system response, $[G]$ includes the sliding surface slopes, and $\boldsymbol{e}$ is the state error vector. For stability, the following Lyapunov function candidate, which is proposed for a non-chattering action, must be positive definite and its derivative must be negative semi-definite:

$$\mathbf{v}(\boldsymbol{\sigma}) = \frac{\boldsymbol{\sigma}^T \boldsymbol{\sigma}}{2} > 0 \tag{7}$$

$$\frac{\mathrm{d}\mathbf{v}(\boldsymbol{\sigma})}{\mathrm{d}t} = \frac{\dot{\boldsymbol{\sigma}}^T \boldsymbol{\sigma}}{2} + \frac{\boldsymbol{\sigma}^T \dot{\boldsymbol{\sigma}}}{2} \leq 0. \tag{8}$$

If the limit condition is applied to equation (8), then

$$\frac{\mathrm{d}\boldsymbol{\sigma}}{\mathrm{d}t} = \frac{\mathrm{d}\mathbf{A}(t)}{\mathrm{d}t} - [G]\frac{\mathrm{d}\phi}{\mathrm{d}t} = 0 \tag{9}$$

where

$$\mathbf{A}(t) = [G]\,\phi_r. \tag{10}$$

From equation (3) and equation (5)

$$\frac{\mathrm{d}\mathbf{A}(t)}{\mathrm{d}t} - [G]\left(\mathbf{f}(\phi) + [B]\ \mathbf{u}_{eq}\right) = 0 \tag{11}$$

where $\mathbf{u}_{eq}$ is the equivalent control torque input vector for the limit case. Finally, the equivalent control is

$$\mathbf{u}_{eq}(t) = [GB]^{-1}\left(\frac{\mathrm{d}\mathbf{A}(t)}{\mathrm{d}t} - [G]\,\mathbf{f}(\phi)\right). \tag{12}$$

Equivalent control is valid only on the sliding surface. Thus, an additional term should be defined to pull the system to the surface. For this purpose, the derivative of the Lyapunov function can be chosen to be

$$\dot{\mathbf{v}} = -\boldsymbol{\sigma}^T\,[\Gamma]\,\boldsymbol{\sigma} < 0. \tag{13}$$

By carrying out necessary calculations, total control input is found to be

$$\mathbf{u}(t) = \mathbf{u}_{eq}(t) + [GB]^{-1}\,[\Gamma]\,\boldsymbol{\sigma} \tag{14}$$

$[GB]^{-1}$ is always pseudo-inverse and equal to the mass matrix for mechanical systems. $[\Gamma]$ is a positive definite matrix, and the values of its terms are decided by trial and error at the design stage. However, if the knowledge of $\mathbf{f}(\phi)$ and $[B]$ are not well known, the calculated equivalent control inputs will be completely different from the actual equivalent control inputs. Thus, in this study, it is assumed that the equivalent control is the average of the total control. For estimation of the equivalent control, an averaging filter, here a low pass filter, can be designed as follows:

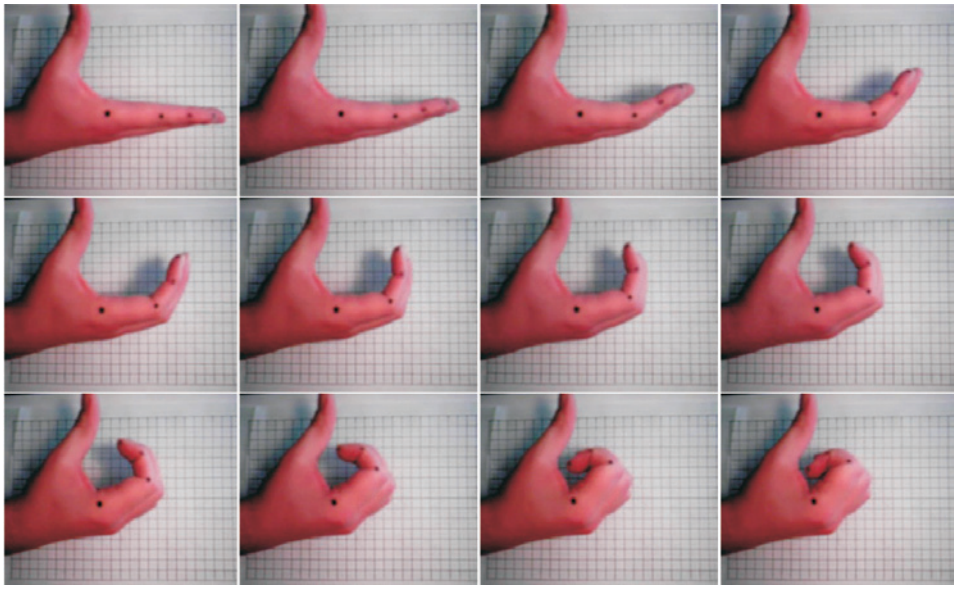

Figure 5. Some of the camera images of the closing motion of the hand.

$$\hat{\mathbf{u}}_{eq}(t) = \frac{1}{Ts+1}\mathbf{u}(t-\delta t) \tag{15}$$

where δt is the sampling time and T is the time constant of the first order low-pass filter. The main idea of designing a low pass filter is that low frequencies determine the characteristics of the signal and high frequencies come from unmodeled dynamics. Finally, the non-chattering control input gives

$$\mathbf{u}(t) = \hat{\mathbf{u}}_{eq}(t) + [GB]^{-1}[\Gamma]\boldsymbol{\sigma}. \tag{16}$$

4. TRAJECTORY PLANNING AND RESULTS

Trajectory planning is an important stage in the kinematic analysis of a prosthetic finger model, since it is supposed to mimic the natural movements of the human finger. In this study, the flexion movement of the index finger of a human hand is investigated. For this purpose, the movement of the human hand while the fingers are closing was recorded using a digital camera. The recorded video was split into frames at 0.08 second intervals; some of these are shown in Figure 5. These frames were then transferred to a computer aided design program where the joint angles were measured with the aid of the marks placed on the finger joints before recording.

In order to have continuous reference paths for the joint angles, sixth order polynomials were fitted to the experimental data. The experimental data and their polynomial approxima-

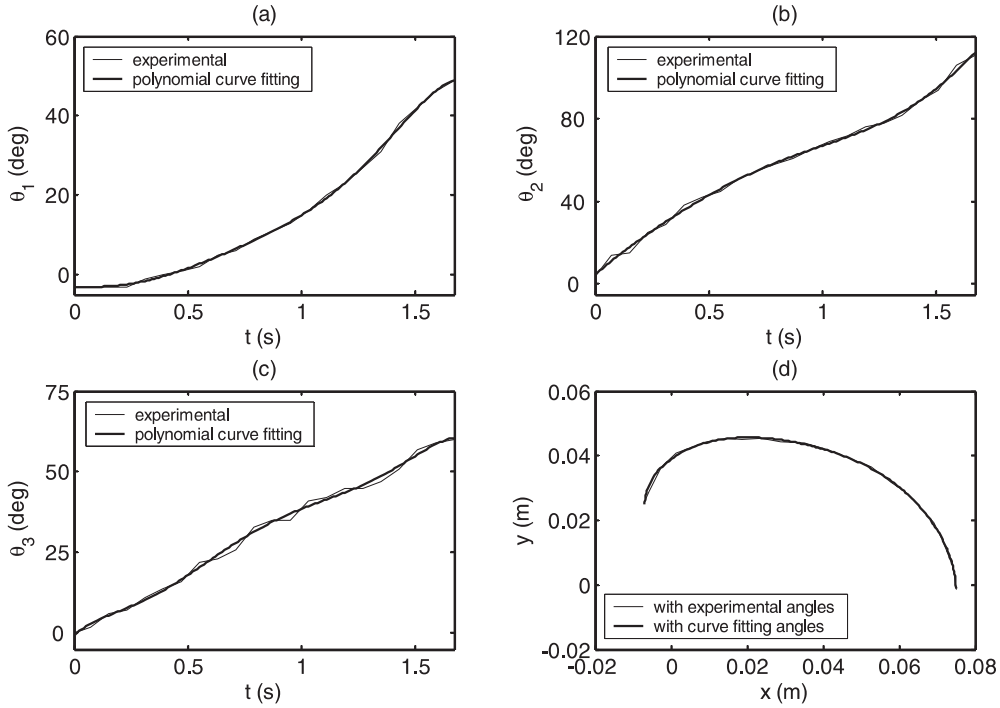

Figure 6. Experimental and approximated reference values for the a) proximal phalange, b) middle phalange, c) distal phalange, and d) reference trajectory of the finger tip.

tions are shown in Figure 6. Using the polynomials as a reference, the motion of the end of the distal link is obtained as given in Figure 6d. These polynomials will be used as reference joint motions for the sliding mode controller.

It should be noted that during numerical analysis, an unexpected joint friction fault is deliberately introduced at the PIP joint after half a second, to test the robustness of the controller:

$$T_r = \mu \text{sign}(\dot{\theta}_2) \tag{17}$$

Where μ is the resistive friction constant, as shown in Figure 7. Numerical parameters for the controller are given in Appendix C.

In Figure 8, the references for the joint angles and tracking errors of the related links are given. It can be seen from this figure that each joint of the finger tracks the specified trajectory successfully in spite of the unexpected joint friction fault, which indicates the efficiency and robust behavior of the sliding mode controller. It can be calculated from Figure 8b that the maximum magnitudes of the error values are 0.8° for the PIP and DIP joints, and less than 0.1° for the MCP joint.

In Figure 9, the reference and resultant trajectories of the finger tip are presented. The tendon forces are shown in Figure 10. Generalized torques are the output signals of the

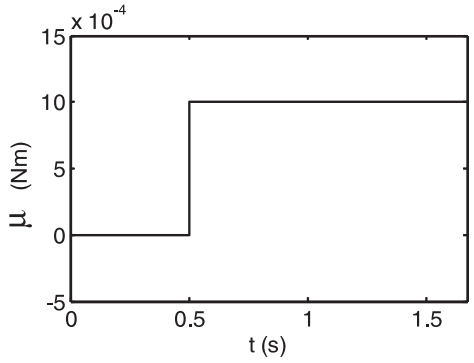

Figure 7. Resistive torque applied to the PIP joint.

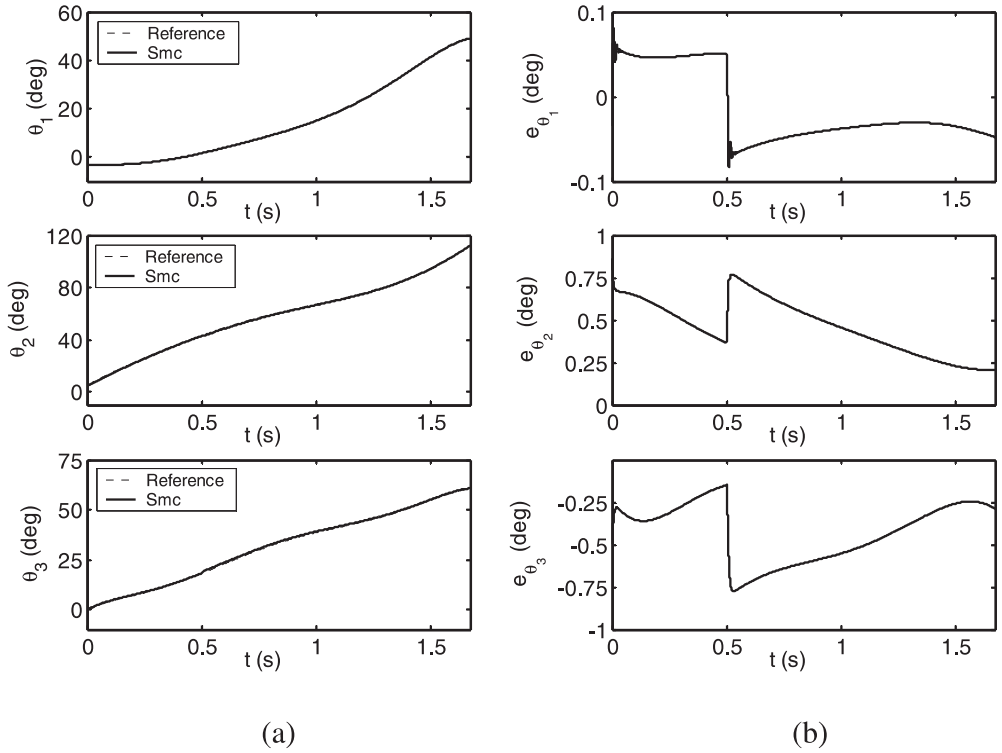

Figure 8. a) Reference and actual values for the links. b) Tracking errors for the links.

controller and tendon forces, which are used to manipulate the finger, and are obtained from these torques as described in Section 2.2. Since the muscles exert only a pulling force on the phalanges, the negative tendon force values in the figure represent inactivity of the flexor tendons in combination with activity of the opposite set of muscles. From the results, it can be seen that maximum tendon forces are obtained for the tendon which actuates the proximal

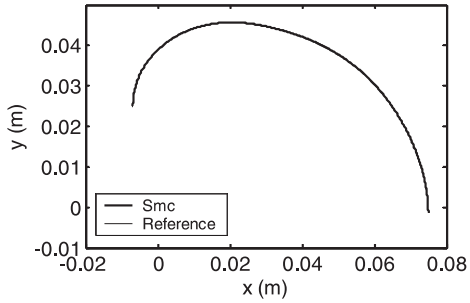

Figure 9. The reference and resultant trajectories of the finger tip.

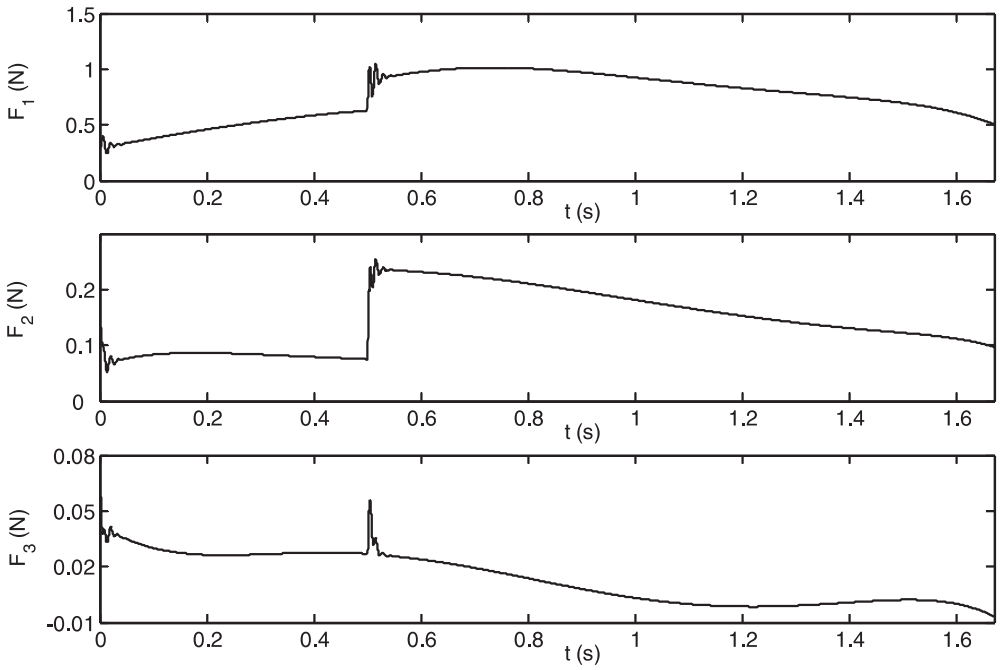

Figure 10. Tendon forces.

phalange and the minimum force was obtained for the tendon of the distal phalange, as expected.

5. CONCLUSION

In this study a prosthetic finger model which resembles the index finger of the human hand was proposed. First, trajectory planning was determined by recording the movements of the human hand in a closing motion. The joint angles desired for performing such a motion were

obtained with the aid of a computer aided design program. Second, the equations of motion of the finger model and the relations between the generalized torques and tendon forces were obtained. Then, a non-chattering robust sliding mode control was used to produce the correct tendon forces to follow the desired trajectory. Numerical results showed that by using the sliding mode controller, an efficient tracking performance was obtained, despite an unexpected friction fault. Additionally, the results showed that the presented tendon arrangement and control method allow the finger model to mimic the motion of a real human index finger.

APPENDIX A

The mass matrix, coriolis-centrifugal vector and gravity vector of the motion equations are

$$[M(\theta)] = \begin{bmatrix} A_1 + A_2 + A_3 + 2L_1A_4c_2 + 2cM_3\left(L_1c_{23} + L_2c_3\right) & A_2 + A_3 + L_1A_4c_2 + cM_3\left(L_1c_{23} + 2L_2c_3\right) & A_3 + cM_3\left(L_1c_{23} + L_2c_3\right) \\ A_2 + A_3 + L_1A_4c_2 + cM_3\left(L_1c_{23} + 2L_2c_3\right) & A_2 + A_3 + 2cM_3L_2c_3 & A_3 + cM_3L_2c_3 \\ A_3 + cM_3\left(L_1c_{23} + L_2c_3\right) & A_3 + cM_3L_2c_3 & A_3 \end{bmatrix}$$

$$\mathbf{C}(\theta, \dot{\theta}) = \begin{bmatrix} b_1\dot{\theta}_1 - L_1\left(A_4s_2 + cM_3s_{23}\right)\left(2\dot{\theta}_1\dot{\theta}_2 + \dot{\theta}_2^2\right) - cM_3\left(L_1s_{23} + L_2s_3\right)\left(2\dot{\theta}_1\dot{\theta}_3 + 2\dot{\theta}_2\dot{\theta}_3 + \dot{\theta}_3^2\right) \\ b_2\dot{\theta}_2 + \mu sign(\dot{\theta}_2) + L_1\left(A_4s_2 + cM_3s_{23}\right)\dot{\theta}_1^2 - cM_3L_2s_3\left(2\dot{\theta}_1\dot{\theta}_3 + 2\dot{\theta}_2\dot{\theta}_3 + \dot{\theta}_3^2\right) \\ b_3\dot{\theta}_3 + cM_3\left(\left(L_1s_{23} + L_2s_3\right)\dot{\theta}_1^2 + L_2s_3\left(2\dot{\theta}_1\dot{\theta}_2 + \dot{\theta}_2^2\right)\right) \end{bmatrix}$$

and

$$\mathbf{G}(\theta) = \begin{bmatrix} g\left(A_5c_1 + A_6c_{12} + cM_3c_{123}\right) \\ g\left(A_6c_{12} + cM_3c_{123}\right) \\ gcM_3c_{123} \end{bmatrix}$$

where

$$\begin{aligned} A_1 &= M_1a^2 + I_1 + (M_2 + M_3)L_1^2 \\ A_2 &= M_2b^2 + I_2 + M_3L_2^2 \\ A_3 &= M_3c^2 + I_3 \\ A_4 &= M_2b + M_3L_2 \\ A_5 &= M_1a + (M_2 + M_3)L_1 \\ A_6 &= M_2b + M_3L_2. \end{aligned}$$

Table 1. Numerical parameters for the model.

Parameter	Numerical value	Unit	Parameter	Numerical value	Unit
M_1	0.0090	[kg]	b	0.0091	[m]
M_2	0.0032	[kg]	c	0.0068	[m]
M_3	0.0010	[kg]	a_1	0.0095	[m]
I_1	1.1291×10^{-6}	[kg]	a_2	0.0038	[m]
I_2	1.3303×10^{-7}	[kg]	a_3	0.0027	[m]
I_3	2.3656×10^{-8}	[kg]	t_1	0.0138	[m]
L_1	0.038	[kgm^2]	t_2	0.0113	[m]
L_2	0.021	[kgm^2]	t_3	0.0075	[m]
L_3	0.016	[kgm^2]	β_i	10	[deg]
a	0.0165	[m]	b_i	0.0001	[Nms]

In the expressions above, the abbreviations $c_1 = \cos\theta_1$, $s_2 = \sin\theta_2$, $c_{123} = \cos(\theta_1 + \theta_2 + \theta_3)$, and $s_{23} = \sin(\theta_2 + \theta_3)$ are used.

The numerical parameters used are given in Table 1.

APPENDIX B

$[J]^T$, $\mathbf{F}_c$ and $\mathbf{u}$ are

$$[J]^T = \begin{bmatrix} \frac{\partial x_1}{\partial \theta_1} & \frac{\partial y_1}{\partial \theta_1} & \frac{\partial x_2}{\partial \theta_1} & \frac{\partial y_2}{\partial \theta_1} & \frac{\partial x_3}{\partial \theta_1} & \frac{\partial y_3}{\partial \theta_1} \\ \frac{\partial x_1}{\partial \theta_2} & \frac{\partial y_1}{\partial \theta_2} & \frac{\partial x_2}{\partial \theta_2} & \frac{\partial y_2}{\partial \theta_2} & \frac{\partial x_3}{\partial \theta_2} & \frac{\partial y_3}{\partial \theta_2} \\ \frac{\partial x_1}{\partial \theta_3} & \frac{\partial y_1}{\partial \theta_3} & \frac{\partial x_2}{\partial \theta_3} & \frac{\partial y_2}{\partial \theta_3} & \frac{\partial x_3}{\partial \theta_3} & \frac{\partial y_3}{\partial \theta_3} \end{bmatrix}$$

$$\mathbf{F}_c = \begin{bmatrix} F_{1x} & F_{1y} & F_{2x} & F_{2y} & F_{3x} & F_{3y} \end{bmatrix}^T$$

and

$$\mathbf{u} = \begin{bmatrix} u_1 & u_2 & u_3 \end{bmatrix}^T$$

where

$$x_1 = a_1 \cos\theta_1 - \frac{t_1}{2}\sin\theta_1$$

$$y_1 = a_1 \sin\theta_1 + \frac{t_1}{2}\cos\theta_1$$

$$x_2 = L_1 \cos\theta_1 + a_2 \cos\theta_{12} - \frac{t_2}{2}\sin\theta_{12}$$

$$
\begin{aligned}
y_2 &= L_1 \sin\theta_1 + a_2 \sin\theta_{12} + \frac{t_2}{2}\cos\theta_{12} \\
x_3 &= L_1 \cos\theta_1 + L_2 \cos\theta_{12} + a_3 \cos\theta_{123} - \frac{t_3}{2}\sin\theta_{123} \\
y_3 &= L_1 \sin\theta_1 + L_2 \sin\theta_{12} + a_3 \sin\theta_{123} + \frac{t_3}{2}\cos\theta_{123}
\end{aligned}
$$

where x_i and y_i $(i = 1, 2, 3)$ denote the positions of the attachment points of the flexor tendons to the related phalanges, where $\theta_{12} = \theta_1 + \theta_2$ and $\theta_{123} = \theta_1 + \theta_2 + \theta_3$.

$$
\begin{aligned}
F_{1x} &= F_1 \cos\alpha_1; \quad F_{2x} = F_2 \cos\alpha_2; \quad F_{3x} = F_3 \cos\alpha_3 \\
F_{1y} &= F_1 \sin\alpha_1; \quad F_{2y} = F_2 \sin\alpha_2; \quad F_{3y} = F_3 \sin\alpha_3
\end{aligned}
$$

where α_i $(i = 1, 2, 3)$ are the angles of the flexor tendon forces with respect to the base frame and are defined as

$$
\begin{aligned}
\alpha_1 &= \theta_1 + (\pi - \beta_1) \\
\alpha_2 &= \theta_1 + \theta_2 + (\pi - \beta_2) \\
\alpha_3 &= \theta_1 + \theta_2 + \theta_3 + (\pi - \beta_3).
\end{aligned}
$$

As a result, using equation (2), the tendon forces for the closing action are

$$
\begin{aligned}
F_1 = {} & \left\{ u_1 \left[\left(\frac{t_3}{2}\cos(\alpha_3 - \theta_{123}) - a_3 \sin(\alpha_3 - \theta_{123}) \right) \right.\right. \\
& \times \left.\left. \left(\frac{t_2}{2}\cos(\alpha_2 - \theta_{12}) - a_2 \sin(\alpha_2 - \theta_{12}) \right) \right] \right. \\
& + u_2 \left[\left(\frac{t_3}{2}\cos(\alpha_3 - \theta_{123}) - a_3 \sin(\alpha_3 - \theta_{123}) \right) \right. \\
& \times \left. \left(a_2 \sin(\alpha_2 - \theta_{12}) + L_1 \sin(\alpha_2 - \theta_1) - \frac{t_2}{2}\cos(\alpha_2 - \theta_{12}) \right) \right] \\
& + u_3 \left[L_1 \sin(\alpha_2 - \theta_1) \left(a_3 \sin(\alpha_3 - \theta_{123}) + L_2 \sin(\alpha_3 - \theta_{12}) - \frac{t_3}{2}\cos(\alpha_3 - \theta_{123}) \right) \right. \\
& + \left. L_1 \sin(\alpha_3 - \theta_1) \left(\frac{t_2}{2}\cos(\alpha_2 - \theta_{12}) - a_2 \sin(\alpha_2 - \theta_{12}) \right) \right] \Bigg\} \\
& / \left\{ \left[\frac{t_3}{2}\cos(\alpha_3 - \theta_{123}) - a_3 \sin(\alpha_3 - \theta_{123}) \right] \left[a_1 \sin(\alpha_1 - \theta_1) - \frac{t_1}{2}\cos(\alpha_1 - \theta_1) \right] \right. \\
& \times \left. \left[\frac{t_2}{2}\cos(\alpha_2 - \theta_{12}) - a_2 \sin(\alpha_2 - \theta_{12}) \right] \right\}
\end{aligned}
$$

$$
\begin{aligned}
F_2 &= \left\{ u_2 \left[a_3 \sin(\alpha_3 - \theta_{123}) - \frac{t_3}{2} \cos(\alpha_3 - \theta_{123}) \right] \right. \\
&+ \left. u_3 \left[\frac{t_3}{2} \cos(\alpha_3 - \theta_{123}) - a_3 \sin(\alpha_3 - \theta_{123}) - L_2 \sin(\alpha_3 - \theta_{12}) \right] \right\} \\
&/ \left\{ \left[a_2 \sin(\alpha_2 - \theta_{12}) - \frac{t_2}{2} \cos(\alpha_2 - \theta_{12}) \right] \left[a_3 \sin(\alpha_3 - \theta_{123}) - \frac{t_3}{2} \cos(\alpha_3 - \theta_{123}) \right] \right\}
\end{aligned}
$$

and

$$
F_3 = u_3 \Big/ \left[a_3 \sin(\alpha_3 - \theta_{123}) - \frac{t_3}{2} \cos(\alpha_3 - \theta_{123}) \right].
$$

If extension motion of the fingers is considered, then the extension forces F_1', F_2', F_3' are obtained similarly:

$$
\begin{aligned}
x_1' &= a_1 \cos\theta_1 + \frac{t_1}{2} \sin\theta_1 \\
y_1' &= a_1 \sin\theta_1 - \frac{t_1}{2} \cos\theta_1 \\
x_2' &= L_1 \cos\theta_1 + a_2 \cos\theta_{12} + \frac{t_2}{2} \sin\theta_{12} \\
y_2' &= L_1 \sin\theta_1 + a_2 \sin\theta_{12} - \frac{t_2}{2} \cos\theta_{12} \\
x_3' &= L_1 \cos\theta_1 + L_2 \cos\theta_{12} + a_3 \cos\theta_{123} + \frac{t_3}{2} \sin\theta_{123} \\
y_3' &= L_1 \sin\theta_1 + L_2 \sin\theta_{12} + a_3 \sin\theta_{123} - \frac{t_3}{2} \cos\theta_{123}.
\end{aligned}
$$

Here, x_i' and y_i' $(i = 1, 2, 3)$ denote the positions of the attachment points of the extensor tendons to the related phalanges.

$$
\begin{aligned}
F_{1x}' &= F_1' \cos\alpha_1'; \quad F_{2x}' = F_2' \cos\alpha_2'; \quad F_{3x}' = F_3' \cos\alpha_3' \\
F_{1y}' &= F_1' \sin\alpha_1'; \quad F_{2y}' = F_2' \sin\alpha_2'; \quad F_{3y}' = F_3' \sin\alpha_3'
\end{aligned}
$$

where α_i' $(i = 1, 2, 3)$ are the angles of the extensor tendon forces with respect to the base frame and

$$
\begin{aligned}
\alpha_1' &= \theta_1 + (\pi + \beta_1) \\
\alpha_2' &= \theta_1 + \theta_2 + (\pi + \beta_2) \\
\alpha_3' &= \theta_1 + \theta_2 + \theta_3 + (\pi + \beta_3).
\end{aligned}
$$

As a result, again using equation (2), the tendon forces for opening action are obtained as

$$
\begin{aligned}
F_1' &= \left\{ u_1 \left[\left(a_3 \sin(\alpha_3' - \theta_{123}) + \frac{t_3}{2} \cos(\alpha_3' - \theta_{123}) \right) \right.\right. \\
&\times \left.\left. \left(a_2 \sin(\alpha_2' - \theta_{12}) + \frac{t_2}{2} \cos(\alpha_2' - \theta_{12}) \right) \right] \right. \\
&- u_2 \left[\left(a_3 \sin(\alpha_3' - \theta_{123}) + \frac{t_3}{2} \cos(\alpha_3' - \theta_{123}) \right) \right. \\
&\times \left. \left(a_2 \sin(\alpha_2' - \theta_{12}) + L_1 \sin(\alpha_2' - \theta_1) + \frac{t_2}{2} \cos(\alpha_2' - \theta_{12}) \right) \right] \\
&+ u_3 \left[L_1 \sin(\alpha_2' - \theta_1) \left(a_3 \sin(\alpha_3' - \theta_{123}) + L_2 \sin(\alpha_3' - \theta_{12}) + \frac{t_3}{2} \cos(\alpha_3' - \theta_{123}) \right) \right. \\
&- \left. L_1 \sin(\alpha_3' - \theta_1) \left(a_2 \sin(\alpha_2' - \theta_{12}) + \frac{t_2}{2} \cos(\alpha_2' - \theta_{12}) \right) \right] \Bigg\} \\
&/ \left\{ \left[a_3 \sin(\alpha_3' - \theta_{123}) + \frac{t_3}{2} \cos(\alpha_3' - \theta_{123}) \right] \left[a_2 \sin(\alpha_2' - \theta_{12}) + \frac{t_2}{2} \cos(\alpha_2' - \theta_{12}) \right] \right. \\
&\times \left. \left[a_1 \sin(\alpha_1' - \theta_1) + \frac{t_1}{2} \cos(\alpha_1' - \theta_1) \right] \right\} \\
F_2' &= \left\{ u_2 \left[a_3 \sin(\alpha_3' - \theta_{123}) + \frac{t_3}{2} \cos(\alpha_3' - \theta_{123}) \right] \right. \\
&- \left. u_3 \left[a_3 \sin(\alpha_3' - \theta_{123}) + L_2 \sin(\alpha_3' - \theta_{12}) + \frac{t_3}{2} \cos(\alpha_3' - \theta_{123}) \right] \right\} \\
&/ \left\{ \left[a_3 \sin(\alpha_3' - \theta_{123}) + \frac{t_3}{2} \cos(\alpha_3' - \theta_{123}) \right] \left[a_2 \sin(\alpha_2' - \theta_{12}) + \frac{t_2}{2} \cos(\alpha_2' - \theta_{12}) \right] \right\}
\end{aligned}
$$

and

$$
F_3' = u_3 \Big/ \left[a_3 \sin(\alpha_3' - \theta_{123}) + \frac{t_3}{2} \cos(\alpha_3' - \theta_{123}) \right] .
$$

APPENDIX C

Table 2. Numerical parameters of the controller.

$\Gamma_1 = 200$	$\Gamma_3 = 600$
$\Gamma_2 = 400$	$T_i = 0.001$

Acknowledgment. This work is supported by the Research Fund of Istanbul University, Project Number UDP-742/ 11052006.

REFERENCES

Asfour, T., Berns, K., and Dillmann, R., 1999, "The humanoid robot ARMAR," in *Proceedings of the Second International Symposium on Humanoid Robots (HURO '99)*, Tokyo, Japan, October 8–9, pp. 174–180.

Bundhoo, V. and Park, E. J., 2005, "Design of an artificial muscle actuated finger towards biomimetic prosthetic hands," in *Proceedings of the 12th International Conference on Advanced Robotics (ICAR '05)*, Seattle, WA, July 18–20, pp. 368–375.

Cavallo, A. and Natale, C., 2004, "High-order sliding control of mechanical systems: Theory and experiments," *Control Engineering Practice* **12**, 1139–1149.

Craig, J. J., 1989, *Introduction to Robotics: Mechanics and Control*, 2^{nd} Edition, Addison-Wesley, Boston, MA.

Fukaya, N., Toyama, S., Asfour, T., and Dillmann, R., 2000, "Design of the TUAT/Karlsruhe humanoid hand," in *Proceedings of the IEEE/RSJ International Conference on Intelligent Robots and Systems (IROS '00)*, Takomotsu, Japan, October 30 – November 5, pp. 13–19.

Gao, W. and Hung, J. C., 1993, "Variable structure control of nonlinear systems: A new approach," *IEEE Transactions on Industrial Electronics* **40(1)**, 45–55.

Gray, H., 1958, *Gray's Anatomy: Descriptive and Surgical*, http://en.wikipedia/wiki/Grays_Anatomy (accessed February 22, 2007).

Gregory, R. W., 2002, "Biomechanics and control of torque production during prehension," Ph.D. Thesis, Pennsylvania State University, PA.

Hristu, D., Babb, J., Singh, H., and Gottschlich, S., 1994, "Position and force control of a multifingered hand: A comparison of fuzzy logic to traditional PID control," in P*roceedings of the IEEE/RSJ/GI International Conference on Intelligent Robots and Systems (IROS '94)*, September 12–16, pp. 1391–1398.

Jacobsen, S. C., Ko, H., Iversen, E. K., and Davis, C. C., 1990, "Control strategies for tendon-driven manipulators," *IEEE Control Systems Magazine* **10(2)**, 23–28.

Jones, L., 1997, "Dextrous hands: Human, prosthetic and robotic: A survey," *Presence: Teleoperators and Virtual Environments* **6(1)**, 29–56.

LaViola, J. J., Jr., 1999, "A survey of hand posture and gesture recognition techniques and technology," *Technical Report CS-99-11*, Department of Computer Science, Brown University, Providence, RI.

Kawanishi, K., Hashizumi, H., Oki, Y., Nakano, Y., Fukuda, T., Vachkov, G., Arai, F., and Hasegawa, Y., 2000, "Position and elasticity control for biomimetic robot finger," in *Proceedings of the 26th Annual Conference of the IEEE Industrial Electronics Society (IEKON '00)*, Nagoya, Japan, October 22–28, pp. 870–875.

Li, Z. M., Zatsiorsky, V. M., and Latash, M. L., 2000, "The effect of extensor mechanism on finger flexor force," in *Proceedings of the 24th Annual Meeting of the American Society of Biomechanics*, Chicago, IL, July 19–22.

Morita, S., Shibata, K., Zheng X. Z., and Ito, K., 2000, "Prosthetic hand control based on torque estimation from EMG Signals," in *Proceedings of the IEEE/RSJ International Conference on Intelligent Robots and Systems (IROS '00),* Tokyo, Japan, October 30–November 5, pp. 389–394.

Morita, S., Kondo, T., and Ito, K., 2001, "Estimation of forearm movement from EMG signal and application to prosthetic hand control," in *Proceedings of the IEEE International Conference on Robotics and Automation (ICRA '01)*, May 21–26, Seoul, South Korea, pp. 3692–3697.

Pollard, N. and Gilbert, R.C., 2002, "Tendon arrangement and muscle force requirements for humanlike force capabilities in a robotic finger," in *Proceedings of the IEEE International Conference on Robotics and Automation (ICRA '02)*, Washington, DC, May 11–15, pp. 3755–3762.

Rohling, R. N. and Hollerbach, J. M., 1994, "Modeling and parameter estimation of the human index finger," in *Proceedings of the IEEE International Conference on Robotics and Automation (ICRA '94)*, San Diego, CA, May 8–13, pp. 223–230.

Slotine, J. J. and Sastry, S. S., 1983, "Tracking control of nonlinear systems using sliding surfaces, with application to robot manipulators," *International Journal of Control* **38(2)**, 465–492.

Tsang, W., Singh, K. and Fiume, E., 2005, "Helping hand: An anatomically accurate inverse dynamics solution for unconstrained hand motion," in *Proceedings of the Eurographics / ACM SIGGRAPH Symposium of Computer Animation (SCA 2005)*, Los Angeles, CA, July 29–31, pp 319–328.

Utkin, V. I., 1977, "Variable structure systems with sliding modes," *IEEE Transactions on Automatic Control* **22**, 212–222.

Weghe, M. V., Rogers, M., Weissert, M., and Matsuoka, Y., 2004 "The ACT hand: Design of the skeletal structure," in *Proceedings of the IEEE International Conference on Robotics and Automation (ICRA '04)*, Los Angeles, CA, April 26–May 1, pp. 3375–3379.